Bioconjugate Chemistry

Editors' Choice

pubs.acs.org/bc

Article

Exploring the Potentials of Antibody−siRNA Conjugates in Tumor Cell Gene Silencing without Cationic Assistance

Published as part of Bioconjugate Chemistry special issue "Early Career Innovators in Bioconjugate Chemistry."

Yahui Liu, Yanan Quan, Qi Mao, Ruolin Xu, and Wanyi Tai*

Cite This: https://doi.org/10.1021/acs.bioconjchem.5c00212

Read Online

ACCESS | Metrics & More | Article Recommendations | Supporting Information

ABSTRACT: Antibody−siRNA conjugates (ARCs) are a type of promising drug modalities for cancer therapy. However, initial reports of ARCs present the gene knockdown effect only in limited tissues (e.g., muscles) or tumors of special targets (e.g., TenB2 and BCMA receptors). To expand the scope to more targets, herein we built structurally defined DAR2 ARCs and examined their effect on targeted gene silencing of tumor cells without cationic assistance. We first evaluated the impact of linker structures and Cys-engineered sites on conjugation efficiency, revealing that the ThioMab conjugation of siRNA is favored by the rigid sulfo-SMCC linker coupling at the HC-A118C site. With an additional anion exchange purification process, reactions of this condition can yield a homogeneous ARC product with DAR close to 2 (DAR: 1.9). We found that ARCs, despite a lack of endosome-disrupting ability, can induce effective gene silencing in multiple types of tumor cells by free uptake. The RNAi potency of ARCs is largely affected by siRNA stability and the time interval of uptake. The maximal mRNA knockdown (70−80%) can be achieved on the fourth day after the uptake of ARC bearing the fully modified siRNAs (Adv ESC mode). The delayed silencing activity, together with the restriction to the stable siRNA, indicates that ARC escape from endosomes is a slow and rate-limiting step, suggesting the importance of siRNA stability and resistance to endosomal degradation in ARC activity. In vivo, the anti-HER2 ARC displays a much-compromised circulatory half-life ($t_{1/2} \sim 8$ h) in mice but can induce gene silencing in HCC1954 xenograft tumors and retard the tumor growth. This study demonstrates the potential of ARCs to treat cancers and other extrahepatic diseases.

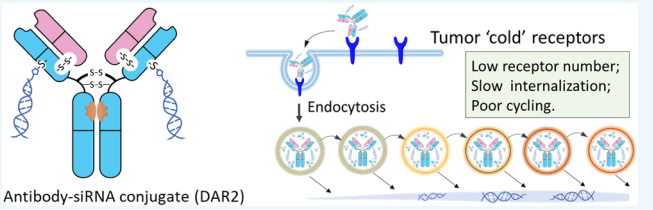

INTRODUCTION

Small interference RNA (siRNA) is a type of short double-stranded RNA molecule that can down-regulate the expression of specific genes by triggering the endogenous RNA interference (RNAi) machinery.[1] Theoretically, siRNA holds tremendous advantages of being able to silence any disease-associated RNA transcripts and its encoded proteins including those "undruggable" ones.[2] Since the groundbreaking discovery of RNAi in the 1990s, siRNA has been embraced as an innovative therapeutic modality that would revolutionize the therapy for many human diseases.[3] The first FDA-approved siRNA is Patisiran, an siRNA-loaded liposome formulation to treat peripheral nerve disease (polyneuropathy), and marketed in August 2018.[4,5] After that, siRNA commercialization goes into a fast track, with almost one drug getting approval per year.[6] Currently, seven siRNAs have been approved by the FDA, and more than 35 candidates are undergoing evaluation in clinical trials.[7] The efficacy and safety of siRNA have been demonstrated in the clinic, but all FDA-approved siRNA drugs solely target the hepatocytes of the liver due to the limitation of current siRNA delivery systems: exclusively hepatic uptake of LNP (i.e., Patisiran) and GalNAc-mediated pathways (i.e., Givosiran, Lumasiran, Inclisiran, Vutrisiran, Nedosiran, and Fitusiran).[8,9] Compared with the hepatic application, siRNA would have clinically widespread use in the treatment of extrahepatic diseases such as cancer. However, targeted delivery of siRNA to extrahepatic tissues remains conceptually complex and challenging.[10]

Given the ability to bind antigens of target cells and their long circulation half-life, monoclonal antibodies are particularly well suited as carriers to deliver siRNAs. The rationale has been bolstered by the clinical successes of antibody−drug conjugates (ADCs), in which chemical toxins are covalently conjugated to antibodies and delivered to tumor cells.[11] However, siRNAs are quite different from chemical toxins in their ability to elicit a therapeutic effect. The small-molecule toxins can easily pass through the cellular membrane and access their targets for blockade. On the contrary, the highly hydrophilic and polyanionic siRNAs are membrane-impermeable. After cellular uptake, they are mostly trapped inside the

Received: May 5, 2025
Revised: June 12, 2025
Accepted: June 17, 2025

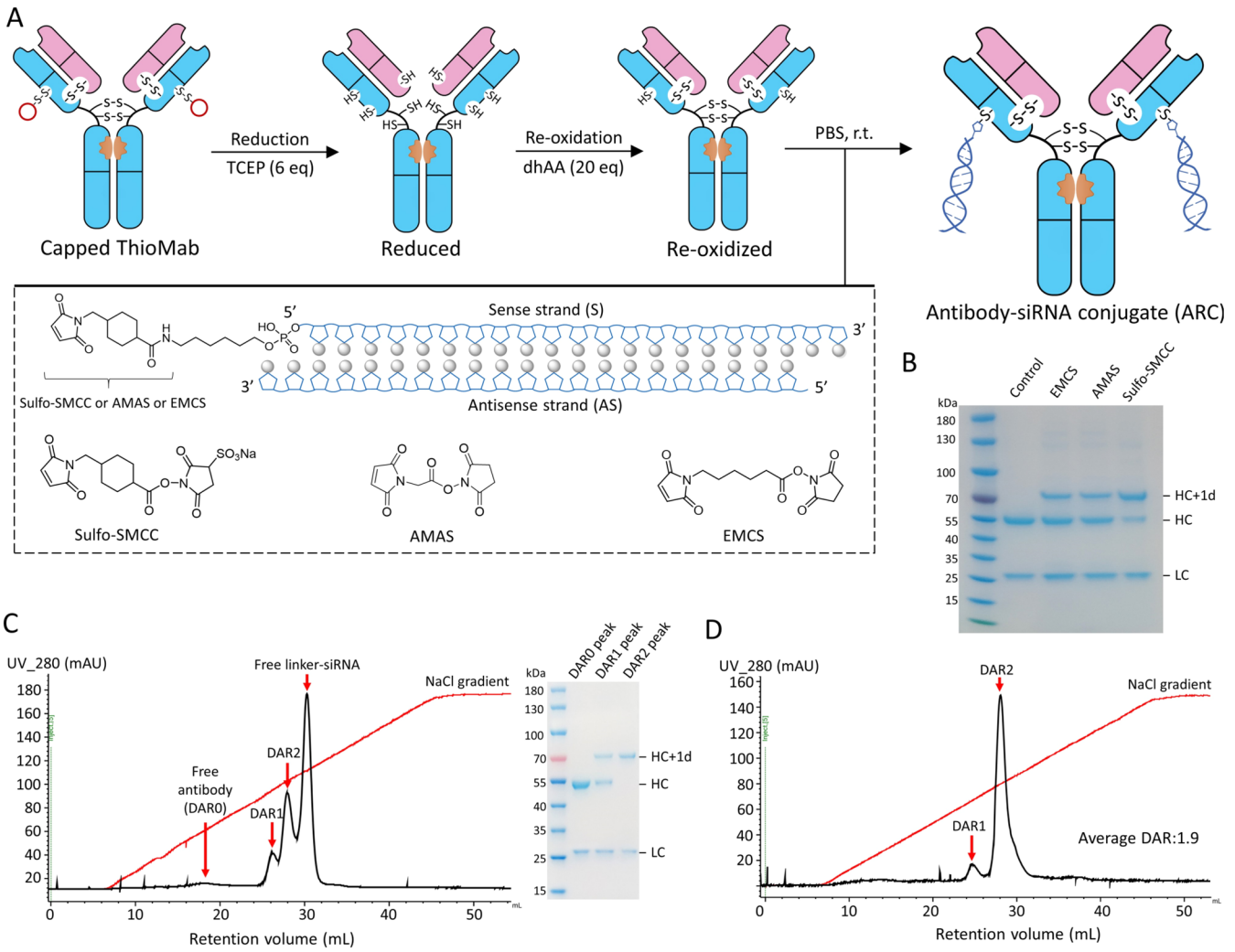

Figure 1. Synthesis of antibody−siRNA conjugates (ARCs). (A) siRNA is reacted with sulfo-SMCC (rigid), AMAS (short), and EMCS (long and flexible) to form a thiol-reactive adduct (maleimide) on the 5′ end of the sense strand. ThioMab (trastuzumab variant HC-A118C) is then activated and conjugated with chemically modified siRNA at the engineered cysteine sites of the heavy chains. The insert box represents the structure of linker functionalized siRNAs. (B) The reduced SDS-PAGE gel image shows the conjugation efficiency of different linkers. (C) Analysis of conjugation reaction by anion exchange chromatography. The ARC peaks are collected and analyzed by an SDS-PAGE gel (right). (D) DAR determination of the purified ARC (DAR2 peak) by anion exchange chromatography. siRNA used for conjugation and purification is the fully modified siPlk1#3.

endosome compartment until complete degradation.[12] To penetrate the endosomal barrier, siRNAs are always codelivered with endosome-disrupting agents (cationic lipids in Patisiran) or take advantage of special uptake pathways such as GalNAc-ASGPR to traverse the endosomal lipid bilayer membrane. In the case of antibody−siRNA conjugates (ARC), the carrier possesses neither cationic components nor special uptake routes, making the delivery extremely challenging.[13]

Schneider et al. developed a bispecific digoxigenin-binding antibody to deliver siRNA to tumor cells but siRNA was not released into the cytosol—unless the cationic transfection agents were supplemented.[14] Ripoll et al. faced a similar problem when they tried to conjugate siRNA with trastuzumab for the targeted delivery to HER2-overexpressing cancer cells.[13] Using the ThioMab approach, Cuellar et al. developed a panel of ARCs across seven different targets.[15] A screen of ARC targets revealed that a subset of ARCs such as anti-TENB2 ARC could induce a moderate silencing to the targeted mRNA, but others including HER2, MUC6, EtBR, etc., despite high copy number per cell, imparted no silencing activity. The study concluded that some receptor−antibody pairs may hijack an unknown pathway to traverse the endosomal barrier. The mechanism is unknown, but all these receptor/antibody pairs seem able to rapidly recycle and turnover after endocytosis, which has a similar feature to the ASGPR/GalNAc pathway. Accordingly, the subsequent studies found that TfR1 is of such type receptors, and ARCs specific to them induce significant mRNA knockdown without the assistance of transfection agents.[16−19] The discovery prompted the development of the first ARC entering the phase 3 clinical trial (NCT06411288, AOC1001 to targeting TfR1 in muscle tissues).[20]

Despite a big leap in siRNA delivery beyond the liver, it is far from reaching the full potential of ARCs. The application of ARCs, so far, has been confined to a limited number of receptor targets. Most other receptors, especially tumor-relevant targets such as HER2, are poor in recycling and turnover, making ARCs targeting them less effective in gene

https://doi.org/10.1021/acs.bioconjchem.5c00212
Bioconjugate Chem. XXXX, XXX, XXX−XXX

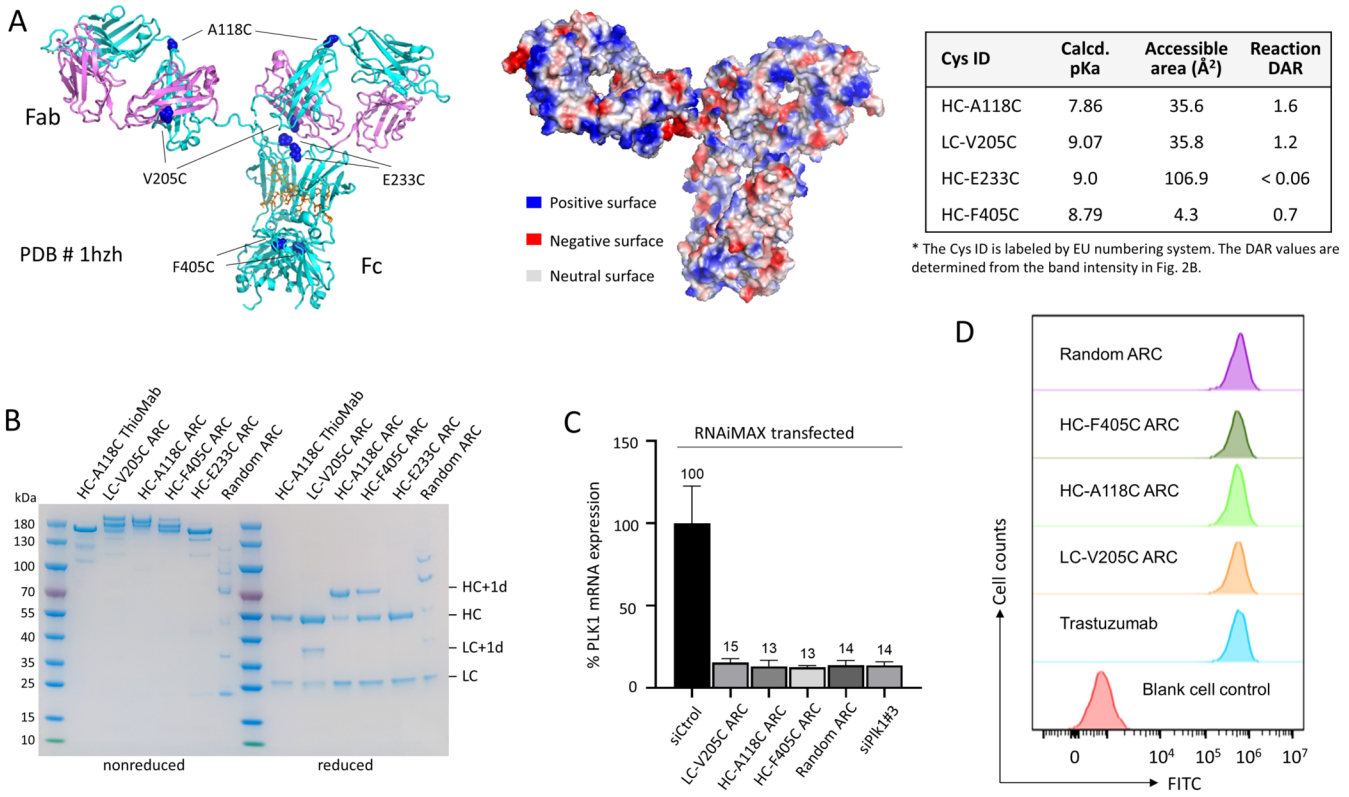

Cys ID	Calcd. pKa	Accessible area (Å²)	Reaction DAR
HC-A118C	7.86	35.6	1.6
LC-V205C	9.07	35.8	1.2
HC-E233C	9.0	106.9	< 0.06
HC-F405C	8.79	4.3	0.7

* The Cys ID is labeled by EU numbering system. The DAR values are determined from the band intensity in Fig. 2B.

Figure 2. Selection of conjugation sites for siRNA by ThioMab approaches. (A) The potential sites for cysteine engineering on human IgG1 antibody. The electrostatic surface of the antibody is shown to analyze the local environment adjacent to conjugation sites. The reactivity of mutated cysteines is predicted and summarized in the table. (B) The SDS-PAGE image to analyze the conjugation reaction in the nonreducing and reducing conditions. Random ARC is obtained by random cysteine conjugation after trastuzumab reduction. siRNA used in reactions is the siPlk1#3. +1d, one drug (siRNA) adduct. (C) The PLK1 silencing effect of ARCs (1 nM, siRNA equivalently) in NCI-N87 cells after transfection by the RNAiMAX reagent. (D) Flow cytometry comparing the binding avidity of the naked anti-HER2 trastuzumab and ARC variants to the HER2-positive NCI-N87 cells.

silencing. In this study, we found that ARCs targeting these tumor receptors can elicit a potent gene silencing effect when siRNA is highly stabilized and the incubation time is extended to 96 h. The rationale might stem from the fact that nuclease-resistant siRNA can prolong the life span in endosomes and increase the escape rate. We demonstrated that the structurally stable ARCs, independent of the receptors they target, can induce effective gene silencing in tumor cells in both in vitro and in vivo. Our results indicate that the chemical stability of siRNA is very important to the bioactivity and endosomal escape of ARCs. By careful optimization of structures, ARCs can be promising gene therapeutics for the treatment of diseases beyond the liver.

RESULTS

ThioMab Conjugation of siRNA Using the Rigid Linker. Figure 1A outlines the synthetic scheme we used to generate the antibody−siRNA conjugate (ARC). It was previously reported that ARC can be prepared by conjugating siRNA with an antibody or its fragment via cysteine, lysine, glutamine, or Asn297.[17] The resulting ARC could be a mixture or relatively homogeneous ARC species, varying with the linker chemistry and purification conditions. We prefer a site-specific conjugation strategy previously reported by Cuellar et al.,[15] which used the cysteine-engineered ThioMab to conjugate siRNAs on heavy chains. Our initial construct employed an anti-HER2 trastuzumab ThioMab, in which two discrete positions were mutated to cysteines (HC-A118C, one per heavy chain) for siRNA coupling. The anti-HER2 ThioMab was cloned, expressed, and purified.[21] To activate the cysteine sites for siRNA conjugation, a typical reduction/oxidization procedure was undergone as reported previously.[22] The two free cysteines were then coupled with siRNAs by the thiol-maleimide chemistry and produced the ARC conjugate in a site-specific manner.

To promote conjugation, siRNA was functionalized by a maleimide adduct. The activated siRNA would react with the free thiol groups of cysteines and covalently link to the antibody via a thioether bond. Owing to the large size and polycharged feature of siRNA, the conjugation is not as efficient as the thiol-maleimide reaction we see in the ADC preparation.[23] Instead, we observed a significant portion of DAR1 species present in the reaction mixture, which is in agreement with the previous reports that conjugation of antibody and siRNA yields ARC with DAR only ∼1.[15,17] To increase the DAR2 output, a screen of linkers was conducted to evaluate the impact of linker length and rigidity on the conjugation efficiency. As shown in Figure 1B, the non-cleavable rigid linker sulfo-SMCC outperformed the flexible linker EMCS and short linker AMAS, producing more DAR2 species. The conjugation reaction was purified using the anion exchange chromatography to remove the free siRNA and DAR1 species (Figure 1C), yielding a homogeneous ARC product with DAR close to 2 (Figures 1D and S1).

https://doi.org/10.1021/acs.bioconjchem.5c00212
Bioconjugate Chem. XXXX, XXX, XXX−XXX

Table 1. Sequence of the Chemically Modified siRNAs in the Study

siRNA	target	modification mode	strand[a]	sequence (5′-3′)	knockdown potency[b]
siPlk1#1	PLK1	Alt OMe, 5′amine	S	5′amine-C6/AGAAGAUGCUUCAGACAGA*T*T	87% (10 nM);
		Alt OMe	AS	UCUGUCUGAAGCAUCUUCU*T*T	88% (1 nM)
					<10% (0.1 nM)
siPlk1#2	PLK1	ESC, 5′amine	S	5′amine-C6/a*G*aAgAuGcuuCaGaCaGaTT	86% (10 nM)
		ESC	AS	U*c*UgUcUgAaGCAuCuUcU*T*T	88% (1 nM)
					<10% (0.1 nM)
siPlk1#3	PLK1	Adv ESC, 5′amine	S	5′amine-C6/A*G*AAGAuGcuuCAGACAGATT	87% (10 nM)
		Adv ESC	AS	U*c*UGUcUGAAGCAuCuUCU*T*T	87% (1 nM)
		Adv ESC, 5′dye	AS		30% (0.1 nM)
					n/a
siPten	Pten	ESC, amine	S	5′amino-C6/a*A*gAuGaUguuUgAaAcUaUu	88% (10 nM)
		ESC	AS	A*a*UaGuUuCaAACaUcAuCuU*G*U	82% (1 nM)
					44% (0.1 nM)
siPPIB	PPIB	Alt OMe, 5′amine	S	5′amino-C6/ACAGCAAAUUCCAUCGUGU*T*T	91% (10 nM)
		Alt OMe	AS	ACACGAUGGAAUUUGCUGU*T*T	89% (1 nM)
					<10%(0.1 nM)
siCtnnb1	CTNNB1	Adv ESC, 5′amine	S	5′amine-C6/U*A*CUGUuGgauUGAUUCGAAA-3′	90% (10 nM)
		Adv ESC	AS	U*u*UCGaAucAAUCcAaCAGUA*G*C	81% (1 nM)
					46% (0.1 nM)
siCtrl	Fluc	Alt OMe, 5′amine	S	5′amine-C6/CUUACGCUGAGUACUUCGA*T*T	n/a
		Alt OMe	AS	UCGAAGUACUCAGCGUAAG*T*T	

[a]S and AS represent sense and antisense strands. Lower-case letters indicate 2′-deoxy-2′-fluoro (2′-F) and underline represents 2′-O-methyl (2′-OMe) ribosugar modifications, respectively. * represents phosphorothioate linkage. n/a, not available. [b]The knockdown potency was obtained by transfecting the indicated concentration of siRNA to HCC1954 cells by the RNAiMAX reagent.

Selection of siRNA Conjugation Sites on Antibody. Besides the linker, the conjugation position on the antibody may play a vital role in determining the yield and stability as well. Based on structural modeling, we selected 4 potential sites (HC-A118C, LC-V205C, HC-E223C, and HC-F405C) for ThioMab engineering and siRNA conjugation (Figure 2A). These cysteine sites differ in the local environments and the thiol (−SH) reactivity, which can be predicted by *in-silico* calculation.[24] HC-A118C and LC-V205C are solvently exposed, and located in the CH1 and CL domains, respectively. HC-E233C is partially buried in the hinge region, and the steric hindrance from Fabs might create obstacles for siRNA conjugation. HC-F405C is located in the CH3 domain and has been used as conjugate sites for ADC STRO-002 and others.[25,26] LC-V205C, HC-E233C, and HC-F405C are all predicted to be surrounded by a positively charged environment. HC-A118C is located in a relatively neutral environment but has the lowest pK_a value in all 4 sites, indicating a better reactivity to the maleimide adduct. To screen these ThioMabs, we incubated an excess amount of SMCC-activated siRNA with all four variants at 37 °C for 2 h and then electrophoresed the reaction mixture on an SDS-PAGE gel. The result in Figure 2B reveals that HC-A118C is the most active site for siRNA coupling. HC-E233C, despite the biggest accessible area, is unable to conjugate siRNAs, likely due to a tendency of forming interchain disulfide bonds by themselves during the reduction/oxidation process. LC-V205C is the second-best of all 4 sites. To explore its potential, we rescreened the linkers on this position and found that the rigid linker sulfo-SMCC remains the best for siRNA coupling (Figure S2). The random conjugates (ARC random), which were generated by coupling siRNA to the reduced Trastuzumab at random sites, can yield high DAR species, but the strategy was abandoned due to the heterogenicity of ARC products.

We then tried to figure out whether the conjugated siRNA retains its silencing activity. The curiosity is intriguing because the covalent attachment to antibodies (∼150 kDa) might interfere with the loading to RNA-induced silencing complex (RISC) and attenuate the siRNA activity. Following the RNAiMAX transfection to tumor cells, we measured the gene knockdown activity of ARCs by real-time quantitative polymerase chain reaction (RT-qPCR) and found that all ARCs, independent of conjugation sites on the antibody (characterized by SEC analysis in Figure S3), are equally active when compared with the free siRNA at the same concentration (Figures 2C and S4). The result is encouraging, and we next examined whether the negatively charged siRNA impairs the ability of antibodies to bind tumor cells. Flow cytometry data (Figures 2D and S5) show that all ARCs bind to the HER2-positive NCI-N87 cells at levels similar to that of the naked antibody (trastuzumab). Collectively, our data demonstrated that siRNA-antibody coupling has no impact on siRNA activity or antibody avidity, no matter what position is selected.

RNAi Efficiency Is Determined by the Stability of Trapped siRNAs against Degradation. Different from other siRNA carriers, antibody possesses no endosome-disrupting moiety. Once uptake, ARC would be trapped inside endosomal compartments until degradation, yielding no gene

https://doi.org/10.1021/acs.bioconjchem.5c00212
Bioconjugate Chem. XXXX, XXX, XXX−XXX

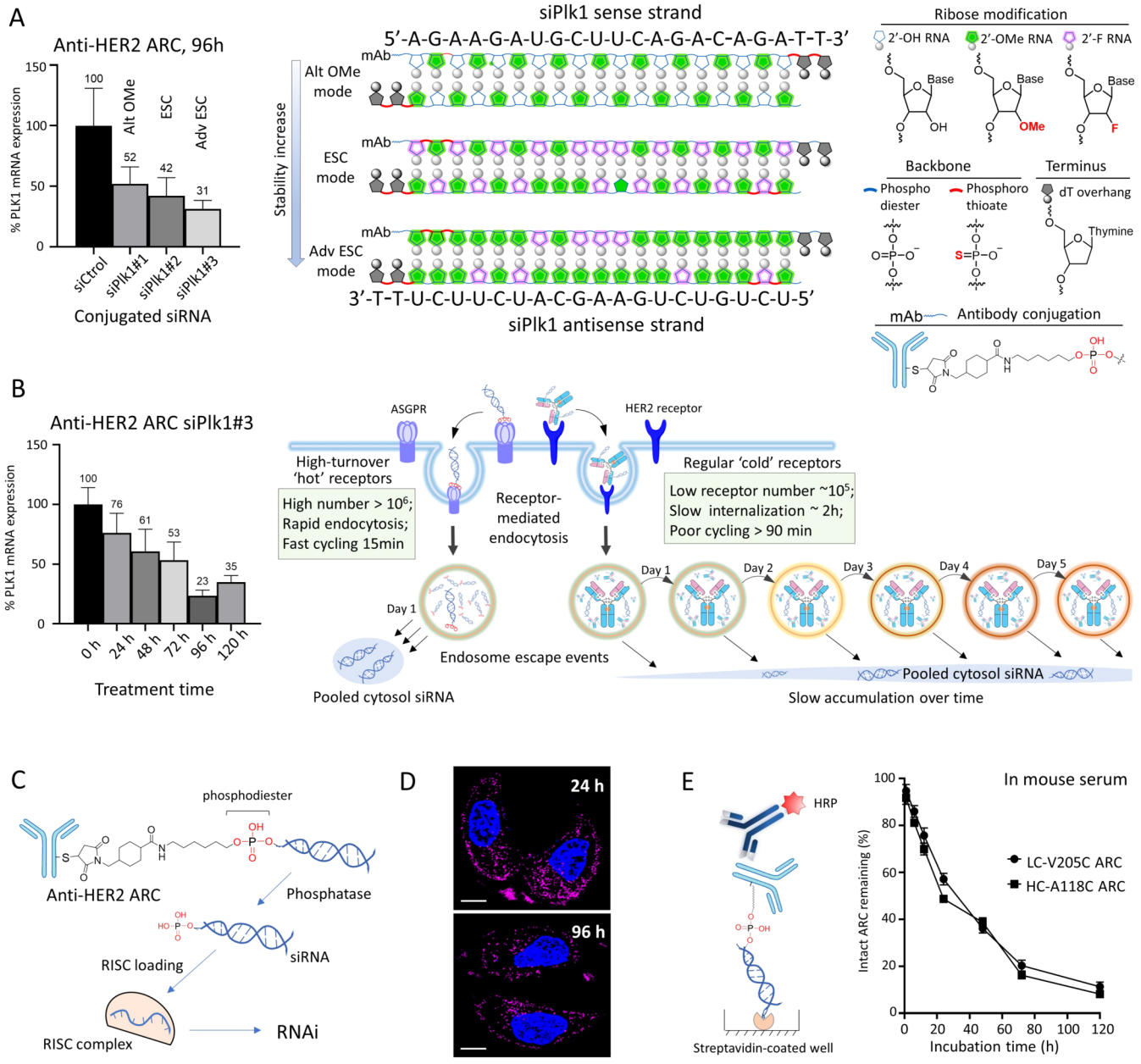

Figure 3. Chemical stability modulates the gene silencing activity and endosomal escape. (A) Anti-HER2 ARCs bearing siRNA of different modification modes produce the variable degree of gene silencing effect dependent on siRNA chemical modification. The assay was performed on NCI-N87 cells at a final concentration of 100 nM ARCs. The modification chemistry includes 2′-O-methyl, 2′-fluoro, phosphorothioate, dT overhang, and antibody covalently linked at the 5′ end of the sense strand by an sulfo-SMCC linker. (B) The time course study to profile the time point of maximal RNAi activity after free uptake of ARC (100 nM) in NCI-N87 cells. The delay of maximal potency indicates a slow siRNA escape from endosomes, which is different from the ASGPR/GalNAc pathway. The "hot" receptors are characterized by the high turnover in receptor trafficking, such as ASGPR receptors in hepatocytes, while the "cold" receptors represent the vast majority which is expressed at a low number, internalized slowly, and recycled poorly. (C) The phosphatase-mediated siRNA release from ARC via the cleavage of phosphodiester linkage. (D) Confocal images to track the free siRNA (sulfo-Cy5 labeled at the antisense strand) in the cytosol. Scale bar: 5 μm. (E) ELISA-based assay to assess the stability of ARC in the mouse serum over time. The phosphate diester linkage could be cleaved by phosphatases in the serum.

silencing effect. However, our group and other laboratories all observed a very minor RNAi effect in cells treated by siRNA conjugates, indicating the presence of siRNA escape events during the endosomal entrapment.[27,28] It is postulated that the trapped siRNA might occasionally leak into the cytosol during the endosome sorting and trafficking, which is likely an inherent error of cell biology.[15,29] The occasional error in sorting, although it happens at a very low frequency, can help ARC traverse the endosomal barrier.[30] We hypothesize that these endosomal escape events might be enriched by increasing the siRNA stability against degradation, thus prolonging its lifetime in endosomes and enhancing the rate of escape. To test this hypothesis, we synthesized anti-HER2 ARCs containing PLK1-specific siRNAs (siPLK1) of different modification modes: Alt OMe (alternated 2′-O-methylation),[31] ESC (enhanced stabilization chemistry),[32] and Adv ESC (advanced ESC) (Table 1).[33] The varying degree of stability is reflected by the base numbers being modified and

https://doi.org/10.1021/acs.bioconjchem.5c00212
Bioconjugate Chem. XXXX, XXX, XXX−XXX

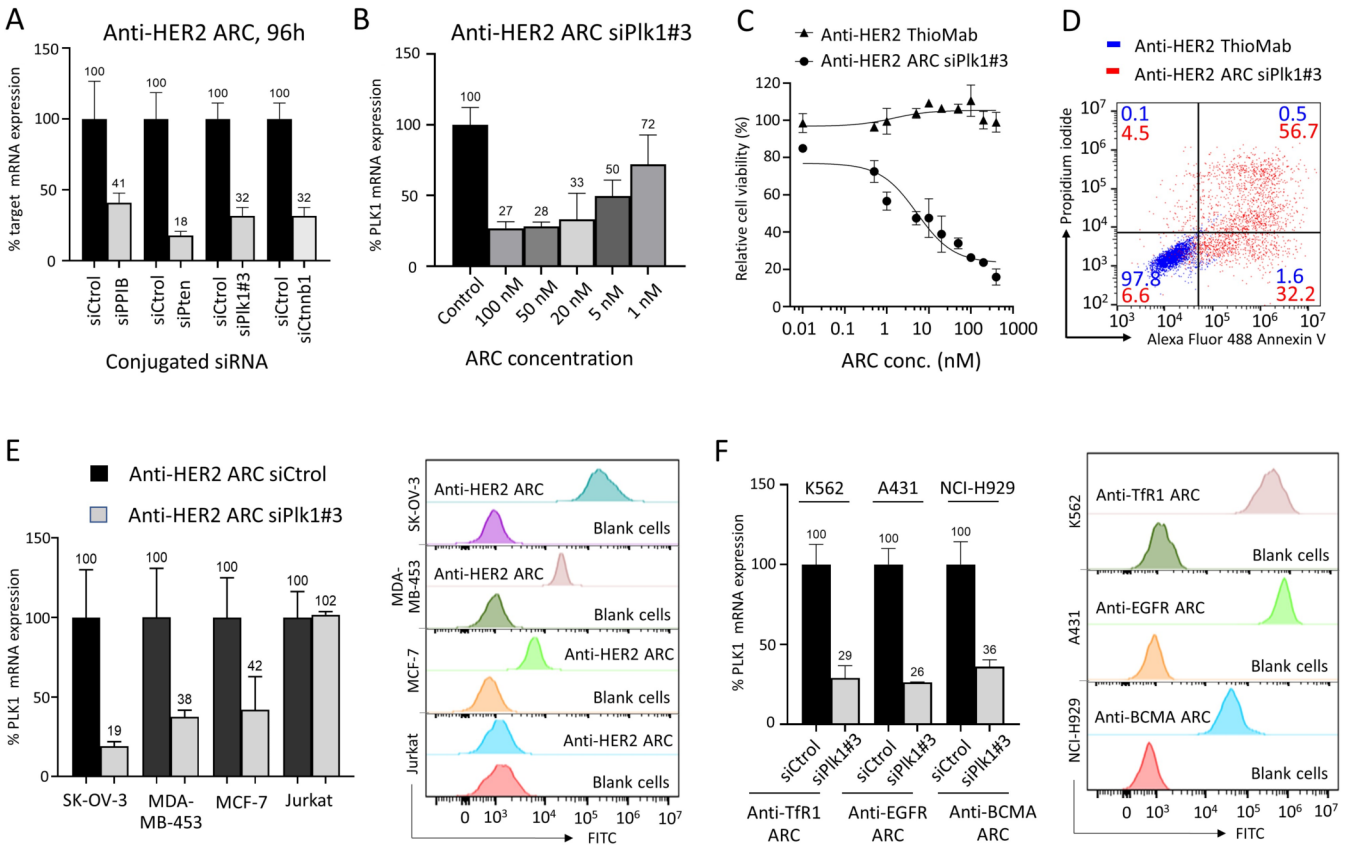

Figure 4. Gene silencing across tumor cells and targets. (A) The delivery of the fully modified siRNAs by anti-HER2 ARCs (100 nM) to knock down Pten, CTNNB1, and PLK1 mRNA, respectively. (B) A dose-responsive assay to reveal the correlation between gene silencing effect and ARC concentration. (C) Cytotoxicity induced by anti-HER2 ARC siPlk1#3 in the sensitive HCC1954 cells. (D) The flow cytometry to analyze apoptosis of HCC1954 cells treated by anti-HER2 ThioMab or ARC (200 nM). (E) The RNAi activity of anti-HER2 ARCs (100 nM) is selective for the HER2-expression status of host cells. (F) The effective delivery of anti-PLK1 siRNA to tumor cells by ARCs (100 nM) targeting different antigens. The antigen-expression levels of tumor cells are plotted against the corresponding ARCs at 50 nM by flow cytometry.

the corresponding ribose chemistry in siRNA backbones (Figure 3A). It is known that 2′-OMe, owing to the sterically demanding substituent, has a greater stabilizing effect than the less bulky modification 2′-F.[34] Accordingly, the Adv ESC mode represents the most stable modification, which we expect to have the longest lifetime in endosomes and may confer the best gene silencing activity. As shown in Figure 3A, we observed an enhancement of RNAi effects along with an increase of siRNA stability. For example, the most stable ARC siPlk1#3 (Adv ESC mode) exhibits a 21% higher knockdown effect than the less stable ARC siPlk1#1 (Alt OMe mode).

We also noticed that the free uptake of ARCs achieves its maximal knockdown at a time point of ∼96 h (Figure 3B), which is much later than the GalNAc-siRNA route (∼24 h) previously reported.[35] It is speculated that GalNAc-siRNA can bind to the liver ASGPR and induces endocytosis in a high number, rapid turnover, and recyclable manner.[30] This uptake mode leads to a rapid accumulation of vast numbers of siRNAs inside endosomes. Despite a tiny endosomal escape rate (<0.01%), ASGPR could bring a burst release of siRNA into the cytosol, resulting in a prompt RNAi effect (Figure 3B, right panel). Most surface receptors in tumor cells, such as HER2, belong to the regular “cold” receptors which have a lower receptor number, slower endocytosis, and poorer cycling efficiency. Consequently, ARCs targeting these “cold” receptors have a smaller number of siRNAs being endocytosed, so fewer siRNAs can escape into the cytosol at the beginning. However, chemically modified siRNA can survive for a long time in acidic endosomes. The trapped siRNA can slowly traverse the endosomal barrier and accumulate in the cytosol, which finally leads to a prominent RNAi effect at the appropriate time, as we see in Figure 3B. It is worth noting that a much higher ARC concentration (100 nM) is required for effective gene silencing by ARCs targeting “cold” receptors than GalNAc-siRNA (as low as 5 nM) to the “hot” ASGPR.[35] Nevertheless, the collective analysis reveals that endosome escape efficacy is determined by both the trapped siRNA number and the lifetime in the endosomes. By increasing the DAR value and siRNA stability, we may obtain a potent ARC for cancer therapy.

Although chemical stability is important during endosomal escape, an unstable phosphodiester linkage in ARCs might be helpful for the payload release and RNAi activity (Figure 3C). It was reported that GalNAc-siRNA conjugates can undergo cleavage of the phosphodiester linker (linkage between hydroxyprolinol and 3′-phosphate of sense strand) in <4 h after liver uptake.[36] Owing to the presence of phosphatases or glycosidases in the cytosol, ARCs might be metabolized to liberate the free siRNA that has no hindrance for RISC loading. To monitor the linker cleavage in the cytosol, we tried to track free siRNA (sulfo-Cy5 labeled) by confocal microscopy. However, the fluorescent signal of cytosol siRNAs is too weak to be detected even after 96 h uptake, likely owing to the low escape efficiency from endosomes (Figure 3D). It

https://doi.org/10.1021/acs.bioconjchem.5c00212
Bioconjugate Chem. XXXX, XXX, XXX−XXX

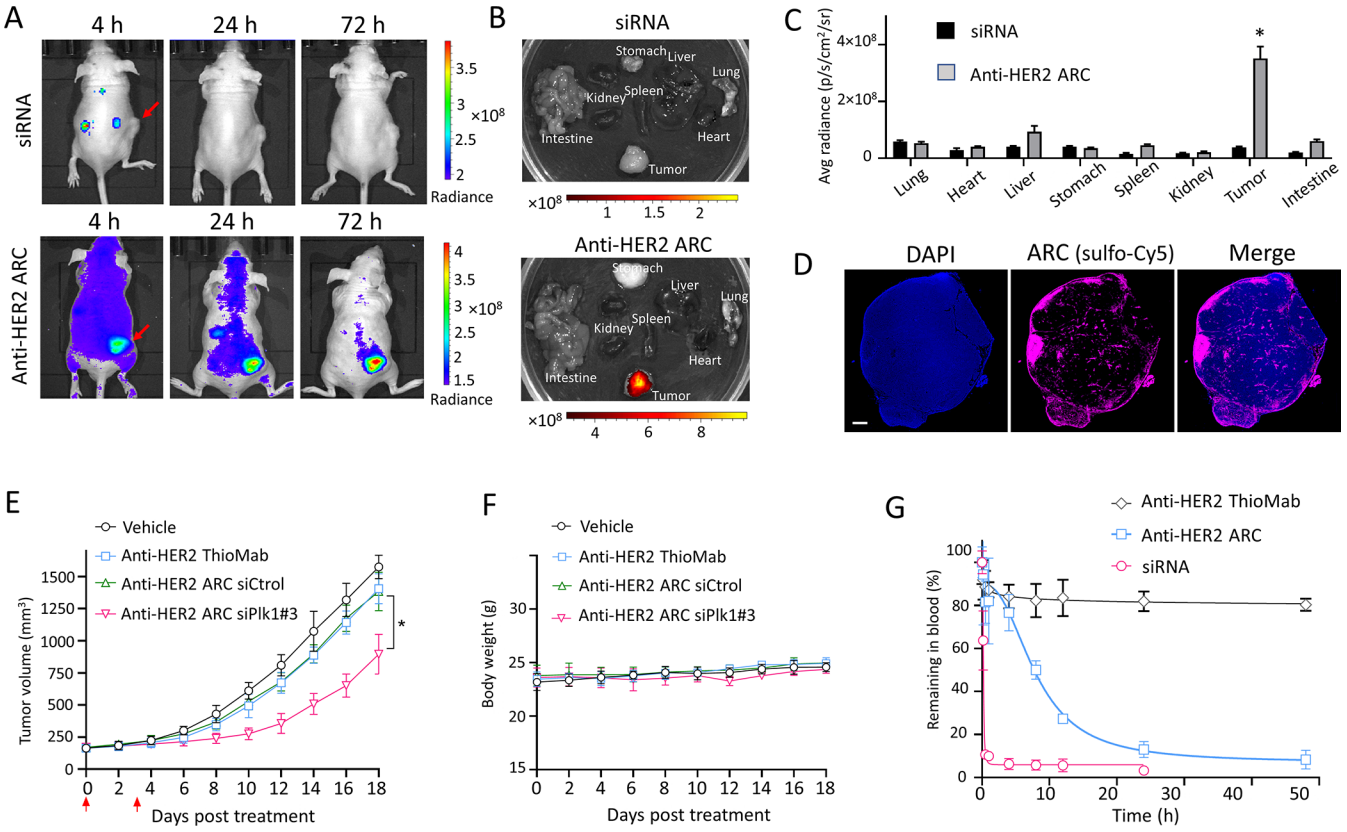

Figure 5. Systemic delivery of siRNA to HCC1954 xenograft tumors by anti-HER2 ARCs. (A) The distribution of sulfo-Cy5-labeled siRNA in mice treated by anti-HER2 ARC. The red arrows point at the tumor sites. (B) The NIR images of tumors and dissected organs at 72 h post administration. (C) Quantification of fluorescence radiance in tissues. (D) Visualization of the ARC penetration in tumor sections. Scale bar, 1 mm. (E) Tumor growth curves after treatment by PBS vehicle control, ThioMab, anti-HER2 ARCs bearing siCtrol or siPlk1#3 siRNAs. The drugs were administrated at the red arrow-indicated time points by the tail-vein route (20 mg/kg). *, $P < 0.05$. (F) The body-weight fluctuation of mice in the antitumor study. (G) Pharmacokinetics of ARC in mice compared with the free siRNA and parent ThioMab antibody.

was reported that the siRNA release from endosomal compartments is restricted to only a limited number of copies (a few hundreds), which is undetectable by standard fluorescence microscopy methods.[37] The lack of efficient methods to track siRNA release from endosomes prevents the testing of this hypothesis.

The linker instability also raises a concern about the premature siRNA release from ARC during delivery. To evaluate the likelihood, we first tested the stability of ARC in PBS for 2 weeks. The SDS-PAGE gel analysis in Figure S6 demonstrated that ARC is quite stable in PBS. We then measured its stability in the mouse serum. In this assay, the ARC integrity was examined by a sandwich ELISA approach, as depicted in Figure 3E.[38] Briefly, ARC was immobilized to the streptavidin-coated well via biotins tagging on the siRNA (antisense strand). During the ELISA assay, only the intact ARC can be detected by the anti-human secondary antibody and produce a horseradish peroxidase (HRP) response. The ELISA data revealed that ARCs display only moderate stability in the mouse serum ($t_{1/2} \sim 30$ h). The result is in line with the previous report that many phosphatases are present in animal sera.[39] It is worth noting that siRNA, even fully modified by advanced ESC, remains accessible by ribonucleases in mouse serum (Figure S7), but its stability is much higher ($t_{1/2} > 120$ h) than the terminal phosphodiester linkage.

Structurally Stable ARCs Induce Gene Silencing Effect across siRNA Sequences, Cell Lines, and Antibody Targets. The applicability of RNAi by ARCs was further explored to deliver the fully modified siRNAs targeting other genes (siPpib, siPten, and siCtnnb1 in Table 1). The strong RNAi effect was observed on HER2-positive NCI-N87 cells after 96 h free uptake of all 4 ARCs (Figure 4A). We then tittered the potency of anti-HER2 ARC by plotting the RNAi effect against the ARC concentrations. As shown in Figure 4B, ARC elicits the significant gene silencing effect at a concentration as low as 5 nM, and the effect is saturable at 50 nM. The mRNA knockdown result is also in agreement with the Western blotting analysis, which confirms that ARC can trigger the downregulation of PLK1 proteins (Figure S8). The prominent gene silencing of the PLK1 gene encourages us to evaluate its cytotoxicity to the siPlk1-sensitive tumor cell line. Breast cancer cell line HCC1954 was selected and evaluated by the CCK-8 assay. The cellular assay in Figure 4C shows a dose-dependent viability profile to ARC treatment and an IC_{50} value of ~5 nM is achieved after 96 h free uptake. The strong cytotoxicity by ARC also goes with a large population of apoptotic cells, as detected by flow cytometry (Figure 4D).

We then evaluated the impact of antibody targetability on the ARC activity by testing the gene silencing potency in cells of different HER2-expression levels. As shown in Figure 4E, a strong correlation between potency and HER2-expression status of host cells was observed. We then expanded the ARC strategy to carrier antibodies targeting other tumor antigens. The anti-TfR1 antibody Delpacibart, anti-EGFR antibody

https://doi.org/10.1021/acs.bioconjchem.5c00212
Bioconjugate Chem. XXXX, XXX, XXX−XXX

Cetuximab, and anti-BCMA antibody Belantamab were expressed, purified, and conjugated with siPLK1#3. All of the ARCs can bind well to tumor cells and elicit the gene silencing effect as profound as anti-HER2 ARC (Figure 4F).

In Vivo Delivery of ARCs to Tumors. The bioactivity in vitro prompted us to investigate whether ARCs can deliver siRNA to tumors and knock down the target mRNA. We first tracked the biodistribution of ARC in mice harboring the HER2-positive HCC1954 xenografts using a near-infrared (NIR) fluorescence imaging system (Figure 5A). Intravenous injection of anti-HER2 ARC (sulfo-Cy5 labeled on siRNA) results in the sequential deposition of siRNA in tumors over time. The selectivity of ARCs to tumors is further confirmed by the ex vivo NIR images of dissected tissues (Figure 5B) and the quantitative analysis of their fluorescent signals (Figure 5C). Histochemical analysis was undertaken to determine the penetration capability of ARC in tumor sections. As shown in Figure 5D, ARC exposure is limited in the tumor periphery (edge) and vasculature, resulting in a suboptimal and heterogeneous tumor distribution. The poor penetration in tumors is likely attributed to the ARC's large size and high molecular weight, which is also seen by therapeutic antibodies and ADCs.[40−42]

We next determined whether ARC can induce gene silencing in xenograft tumors. A pilot study was performed to determine the administration routes and doses in mice. The result demonstrates that ARC is most effective by intravenous (i.v.) injection of 20 mg/kg (equivalent to a 2 mg/kg siRNA), and a peak knockdown activity can be achieved in tumors at around 2 weeks after administration (Figure S9). Accordingly, a dosing regimen (20 mg/kg, 2 injections) was established to treat BALB/c nude mice bearing HCC1954 xenograft tumors. As shown in Figure 5E, a statistically significant retardation of tumor growth was observed in mice treated by anti-HER2 ARC siPlk1#3, but not in the ARC control and ThioMab-treated groups. No sign of side effects or body weight loss was detected throughout the experiment, indicating a good tolerance to the ARC treatment (Figure 5F).

Finally, a pharmacokinetic (PK) study was conducted to assess the circulatory half-life ($t_{1/2}$) of ARC in mice. Figure 5G shows that the clearance rate of ARC ($t_{1/2} \sim 8$ h) is much higher than that of the naked antibody ($t_{1/2} > 50$ h), but remains slower than the unconjugated siRNA ($t_{1/2} < 0.5$ h). A rapid clearance of ARC has been reported by other groups as well.[17,43] It is proposed that the charged siRNA payloads can interact strongly with plasma and cell surface proteins, thus driving a fast elimination from circulation.[44,45] It is worth noting that the short blood circulation time of ARCs may have a negative impact on the tumor penetration ability compared with the long-acting therapeutic ADCs, considering that the binding site frontier could quickly lose the driving force from the concentration gradient. Accordingly, the balance between pharmacokinetics and drug loading, more specifically the DAR value, is important in the design of ARC scaffolds for solid tumor therapy.

DISCUSSION

The siRNA delivery is quite different from the delivery of chemotherapeutic drugs.[46] The final destination of successful siRNA delivery is the cytosol of the target cells. To achieve effective gene knockdown, siRNA needs to overcome the endosome barrier and reach the cytosol where RNAi takes place. The endosomal system is a billion years of evolutionary defense that traps the exogenous materials including siRNAs and prevents them from invading the inside of cells.[47] To break through the barrier, many endosome-disrupting agents, including cationic lipids, fusogenic peptides, and proton-sponge chemicals, have been developed to facilitate the cytosol delivery.[48] However, even using the most efficient delivery systems (i.e., Patisiran LNP and GalNAc conjugates), it was estimated that <2% of the siRNA can escape from endosomes and enter the cytosol.[37,49] As an emerging delivery system, ARC is highly selective to the target cells, but have no endosome-disrupting function, making the siRNA delivery very challenging. Despite the surveillance by endosomes, it is estimated that a very small amount (<0.01%) of the trapped siRNA conjugates can escape from endosomes to the cytosol without the assistance of other agents.[35,50] The endosome escape mechanism is unknown, but it is likely linked to sorting error in the endosomal recycling pathway. This event happens at an extremely low frequency (∼ once per million), making it a rate-limiting step in delivery.[30] It is exemplified by the well-known GalNAc-siRNAs, anti-TfR1 ARCs, and anti-BCMA ARCs.[51] These siRNA conjugates are endocytosed by the fast recycling "hot" receptors and quickly accumulate inside endosomes in large numbers. The high quantity of siRNA copies in the endosome and the corresponding sorting burden might counterbalance the low error frequency, resulting in the adequate siRNA escaped to trigger the gene silencing.[35] As for most ARCs targeting the tumor "cold" receptors, the escaped siRNAs are too few to elicit an effective gene silencing, making this strategy unpopular in siRNA delivery. By increasing the ARC stability, it raises the possibility of a higher escape rate. The hypothesis is tested by in vitro cell-based models and tumor xenografts in this study.

Recently, scientists from Avidity Biosciences Inc. reported that chemically stabilized siRNAs, for example, terminally modified using lock nucleic acid (LNA) and phosphorothioate (P=S), can elongate the gene silencing activity of anti-TfR1 ARC in muscle tissues from 2 to 8 weeks, indicating that more stable siRNAs can lead to longer durations of silencing.[17] Here, we reported that stable siRNA can benefit the gene silencing potency to tumor cells, when targeted by ARCs without cationic assistance. The stability of ARCs, especially the siRNA modification, could secure siRNA integrity and bioactivity in the endosome for an extended period, which increases its chance of traversing the endosomal barrier. We compared the activity of ARC bearing the same siRNA sequence but different modification modes. The result indicated that the gene silencing effect of ARCs is correlated to the siRNA stability (modification mode). Delivered by the anti-HER2 antibody trastuzumab, the most stable siRNA siPlk1#3 (Adv ESC mode) can suppress the target mRNA expression by 69% in a free-uptake manner (100 nM). Notably, the maximal silencing effect is detected 96 h after ARC treatment, a lot later than the transfected siRNA (∼16 h) and GalNAc-siRNA (24 h). The delayed onset of maximal knockdown compared with others reveals that it takes a much longer time for ARCs to pile up enough cytosolic siRNA copies for potent RNAi.

It is encouraging that anti-HER2 ARC could induce effective gene silencing in solid tumors in vivo. The silencing activity in solid tumors is dose-dependent and time-related. In an elegant study, Cuellar and colleagues utilized an anti-TENB2 antibody to deliver siRNAs specific to PPIB (a housekeeping gene) and achieved a weak silencing activity in xenograft tumors.[15] However, the gene silencing activity was not repeatable when

https://doi.org/10.1021/acs.bioconjchem.5c00212
Bioconjugate Chem. XXXX, XXX, XXX−XXX

siRNA was delivered by the anti-HER2 antibody. It is likely because siRNA they used was only partially modified and unable to survive in the acidic endosomes. In this study, a stable ARC is constructed by conjugating a fully modified siRNA to an anti-HER2 antibody via the ThioMab approach. By optimizing the conjugation modality and purification process, we can generate ARCs of DAR2, which carry more siRNA payloads than ARCs of the previous reports (DAR ∼ 1).

High DAR has a negative impact on the antibody pharmacokinetics in mice. The rapid clearance from blood observed with ARCs is likely caused by the negatively charged siRNA payloads which were reported to interact with plasma proteins and facilitate clearance.[44] The siRNA payloads may also alter the physicochemical properties of antibodies, for example, bigger size and greater negative charge density, which might deactivate the recycling machinery, for example, FcRn interaction and IgG recycling (unpublished data). The phenomenon of rapid clearance with ARCs has been observed and reported by other groups as well.[17] In addition, the ELISA study suggested that the phosphodiester bond connecting the antibody and siRNA might be a limiting factor to the overall stability of ARCs. We speculated that the limited stability of the linker may facilitate the clearance of siRNA in vivo as well. The follow-up study to stabilize the phosphodiester linker may improve the pharmacokinetics of ARCs in mice.

In summary, we have demonstrated that chemical optimization of ARCs, especially siRNA components, enables effective gene silencing across tumor cells. Our data show that a stable ARC can effectively kill tumor cells and inhibit the growth of tumor xenografts in mice. It is worth mentioning that ARCs display a circulatory half-life much shorter than that of conventional antibodies and ADCs. Meanwhile, ARCs produce only a limited tumor penetration depth, resulting in suboptimal tumor exposure. All of these factors might compromise the bioactivity of ARCs in vivo. On the basis of this discovery, we may develop new and improved ARCs in upcoming studies for cancer therapy.

MATERIALS AND METHODS

Materials and Cell Lines. Roswell Park Memorial Institute (RPMI) 1640 medium, fetal bovine serum (FBS), and other cell culture supplementary reagents were purchased from Procell Inc. (Wuhan, China). Union-293 expression medium was purchased from Union-Biotech (Shanghai, China), and PEI MAX was purchased from Polysciences (Catalog 24765). siRNA was synthesized by Biosyntech (Suzhou, China). HCC1954, SK-OV-3, MDA-MB-453, MCF-7, Jurkat, NCI-H929, A431, K562, and NCI-N87 cell lines were maintained in RPMI 1640 medium supplemented with 10% FBS and 1% penicillin/streptomycin at 37 °C in 5% CO_2. HEK 293F cells were a kind gift from Dr. F. Long (Wuhan University, China) and maintained in Union-293 expression medium with shaking at a speed of 110 rpm at 37 °C in 5% CO_2.

Antibody Expression. The heavy and light chains of trastuzumab and trastuzumab mutants HC-A118C, HC-E233C, HC-F405C, LC-V205C (Eu numbering), cetuximab HC-A118C, anti-TfR1 HC-A118C, and anti-BCMA HC-A118C were cloned into an expression vector with dual CMV promoter. During transfection, HEK 293F cells were seeded at a density of 1.5×10^6 cells/mL in fresh Union-293 media. For 100 mL culture, 125 μg of plasmid and 400 μg of PEI MAX were diluted in 5 mL of Opti-MEM, respectively, and then mixed and incubated at 37 °C for 5 min. The mixture was added to the culture with shaking at a speed of 110 rpm at 37 °C in 5% CO_2. Twenty hours later, sodium butyrate was added at a final concentration of 10 mM, and glucose was added at a final concentration of 50 mM. Five days after transfection, the culture was collected, and the antibody was purified with protein A column. The purified protein was exchanged to PBS by a Sephadex G-25 desalting column.

siRNA Conjugation and Purification. For ARC construction, bifunctional linkers (sulfo-SMCC, AMAS, and EMCS) were conjugated to siRNA at the 5′ terminal C6/amine of the sense strand. Briefly, duplex siRNA was diluted with 20 mM $NaHCO_3$ aqueous solution. 50 equivalents of linkers (diluted in DMF) were added to the mixture, and then incubated at room temperature for 4 h. The functionalized siRNA was purified with standard ethanol precipitation (repeat twice to remove the residue free linker) and finally dissolved in DEPC water. To activate ThioMab, trastuzumab and other mutants (except trastuzumab) were reduced with 6 equiv of TCEP at 37 °C for 1 h and then desalted by Sephadex G-25 column to remove TCEP. DHAA was added to a final concentration of 1 mM (20 equivalents) to reoxidize the antibody disulfide bonds. DHAA was removed by a Sephadex G-25 desalting column, and the buffer was exchanged to PBS. To conjugate siRNA with antibody, 2.5 equivalents of linker-siRNA was mixed with the activated ThioMab at r.t. for 2 h. Then, the unwanted species were removed by HiScreen Q HP (Cytiva, Catalog 28950511) ion exchange chromatography, and the purified ARC was exchanged to PBS by Sephadex G-25 desalting column. For trastuzumab ARC generated with the random conjugation method, the linker-siRNA was added to the TCEP-reduced antibody, followed by anion exchange purification.

***In Silico* Prediction of the Engineered Cysteine Reactivity.** The 3D structure of the human IgG1 antibody (PDB ID: 1hzh) is used as the model for prediction. The indicated residue (HC-A118C, LC-V205C, HC-E233C, or HC-F405C) is mutated to cysteines and generates ThioMab models using the UCSF Chimera program (version 1.19). To predict the reactivity of engineered cysteines, we calculated the pK_a value and solvent-accessible area of the thiol group (−SH). The pK_a was predicted using the PROPKA algorithm (version 2.0). The surface accessibility, quantified as the solvent-accessible surface area (Å^2) through geometric calculations, was obtained by ASA online tools (version 1.2, Center for Informational Biology, Ochanomizu University). The lower pK_a value and larger accessible area indicate a higher reactivity for the maleimide adduct.

Anion Exchange Chromatography of ARC. One mg portion of ARC was loaded onto a HiScreen Q HP (Cytiva, Catalog 28950511) anion exchange chromatography column and eluted with a linear gradient from 0 to 100% B at 1 mL/min (buffer A, 20 mM Tris, pH 8; buffer B, 20 mM Tris, 1 M NaCl, pH 8) in 40 min. ARCs were eluted from the column according to their charge status. For example, the unconjugated antibody was eluted first, followed by DAR1 and DAR2 ARC, and free siRNA was eluted last.

Flow Cytometry. NCI-N87 cells (25,000 cells per well) were seeded in 24 wells overnight; the cells were digested with trypsin (Gibco, 15050065) and resuspended in RPMI 1640 medium. The antibody or ARC was added at a concentration of 50 nM. One hour after incubation on ice, the cells were

https://doi.org/10.1021/acs.bioconjchem.5c00212
Bioconjugate Chem. XXXX, XXX, XXX−XXX

washed twice and resuspended in DPBS. FITC conjugated goat anti-human IgG (H + L) (Proteintech, SA00003-12) was added with 1:5000 dilution and the mixture was incubated on ice for 1 h. The cells were washed twice and resuspended in DPBS. The fluorescent intensity of cells was analyzed by CytoFlex S (Beckman) according to the manufacturer's instructions. All data were processed with FlowJo 10.6.2.

Serum Stability Test. The 5′ terminal C6 amine of the sense strand was conjugated by biotin-NHS (Bide pharm, 35013-72-0), and the antisense strand (C6 NH2 at the 5′ terminus) was modified by sulfo-SMCC linker. The sense and antisense strands were purified by standard ethanol precipitation twice, and equivalent conjugated sense and antisense strands were annealed in PBS by boiling the mixture and cooling it to room temperature. Trastuzumab HC-A118C ARC (bearing biotin on siRNA) was constructed as mentioned above. ARC was diluted in fresh mouse serum at a concentration of 10 μg/mL, and samples were collected at the indicated time points (1, 2, 6, 24, 48, 72, and 120 h). ARC stability was assessed by enzyme-linked immunosorbent assay (ELISA). Briefly, 96 well plate was coated with streptavidin at a concentration of 1 μg/mL, and the plate was blocked with 3% (weight/volume) BSA for 2 h at room temperature. The serum-treated ARC samples were added and incubated at room temperature for 1 h. The plate was washed with TBST three times. Goat anti-human IgG H&L (HRP) (Abcam, ab6858) was added and incubated at room temperature for another 1 h. The plate was washed with TBST three times, and the TMB substrate was added, followed by incubation at 37 °C for 15 min. 0.1 M H_2SO_4 was added to stop the reaction. The absorbance was immediately measured at 450 nm. The intensities of treated samples against the serum-free wells were calculated and used to determine the percent of intact ARC remaining in serum.

Silencing Effect Assay by Real-Time RT-PCR. For gene silencing assay, NCI-N87 cells were seeded into 96 well plates (10,000 cells per well) the day before experiments. ARCs were added to cells at the indicated concentrations and incubated for 96 h. The ARC bearing the antifirefly luciferase siRNA was used as the control group. After 96 h of incubation, the cell was lysed by the TRIzol reagent (Vazyme, R401-01) and total RNA was isolated according to the manufacturer's instructions. RT-qPCR was conducted with the use of HiScript II One Step qRT-PCR SYBR Green Kit (Vazyme, Q221-01), and the procedure was performed on a CFX connect RT-qPCR detection system (Bio-Rad). Data was analyzed with Bio-Rad CFX Maestro 1.1. The relative changes of PLK1, PTEN, CTNNB1, and PPIB gene expression to the housekeeping β-actin were calculated according to the $2^{-\Delta\Delta CT}$ algorithm. The following primer sequences were used in the real-time PCR assay: β-actin forward: 5′-CCTGTACGCCAACACAGTGC-3′, β-actin reverse: 5′-ATACTCCTGCTTGCTGATCC-3′; PLK1 forward: 5′-CCGAGTTATTCATCGAGACCT-CAAGC-3′; PLK1 reverse: 5′-CTTTGGTTGCCAGTC-CAAAATCCC-3′; PTEN forward: 5′-TCCCAGACATGA-CAGCCATC-3′, PTEN reverse: 5′-TGCTTTGAATC-CAAAAACCTTACT-3′; CTNNB1 forward: 5′-AAAATGGCAGTGCGTTTAG-3′; CTNNB1reverse: 5′-TTTGAAGGCAGTCTGTCGTA3′; PPIB forward: 5′-GATGGCACAGGAGGAAAGAG-3′, PPIB reverse: 5′-AGC-CAGGCTGTCTTGACTGT-3′.

Cell Viability Assay. HCC1954 cells were seeded in 96 well plate at the density of 3000 cells per well. Twenty-four hours later, ARCs or antibodies were added into the wells at a final concentration ranging from 400 to 0.01 nM. The plate was returned to the cell culture incubator and incubated for 96 h. The CCK-8 reagent was added to the wells. After 2 h of incubation, the absorbance at 450 nm was measured by an Infinite M Plex microplate reader (TECAN, Switzerland). The cell viability was profiled by GraphPad Prism version 9.3.0.

Cell Apoptosis Assay. HCC1954 cells were seeded in 24 well plate at a density of 50,000 cells per well. Twenty-four hours later, anti-Her2 Thiomab or ARCs were added into the wells at a final concentration of 200 nM. The plate was returned to the cell culture incubator and incubated for another 96 h. The cell apoptosis assay was performed according to the manufacturer's instructions (Thermo Fisher, A10788). All data were processed by FlowJo 10.6.2.

Confocal Imaging. NCI-N87 cells were seeded in confocal dishes; 24 h later, ARC or free siRNA (labeled with sulfo-Cy5 on the antisense strand) was added at the concentration of 50 nM. After incubation at 37 °C in 5% CO_2 for 24 h, Hoechst 33342 (MilliporeSigma, B2261) was added to stain the cell nucleus for 1 h at 37 °C. The cell monolayer was washed twice with RPMI 1640 and imaged with confocal laser scanning microscopy (Leica).

NIR Imaging In Vivo. All of the animal studies were performed in compliance with the guidelines of the Chinese Regulations for the Administration of Affairs Concerning Experimental Animals and the Institutional Animal Care and Use Committee of Wuhan University. The HCC1954 xenograft tumor model was established by subcutaneous injection of HCC1954 cells (5×10^6) to the dorsal of 6-week-old Balb/c-nu mice. When the tumor volume reached 400 mm^3, 100 μg of ARC or equivalent free siRNA (labeled with sulfo-Cy5 on the antisense strand) was intravenously injected to the mice. The biodistribution was imaged using the In-Vivo Xtreme II imaging system (Bruker) at the indicated time points. For ex vivo imaging, organs were dissected and imaged 72 h after injection. The fluorescence intensity of organs was analyzed with Living Image 4.4, and quantified as Avg Radiant Efficiency [p/s/cm^2/sr]/[μW/cm^2]. The tumors were sectioned into 15 μm slices and stained with DAPI. The section images were obtained with a CaseViewer pannoramic scanner (3DHISTECH, Hungary).

Pharmacokinetic Studies. 100 μg portion of sulfo-Cy7-labeled antibody, ARC, or equivalent free siRNA (labeled with sulfo-Cy7 on the antisense strand) was intravenously injected into the BALB/c mice. The blood samples were collected at indicated time points (1 min, 10 min, 30 min, 1 h, 4 h, 8 h, 12 h, 24 h, and 48 h), and the fluorescence intensity was measured by Odyssey DLX (LI-COR). Data were analyzed by Image Studio Lite version 5.2.

Antitumor Studies. The HCC1954 xenograft tumor model was established. The tumor volume size was calculated using the formula length × $width^2/2$. When the tumor volume reached approximately 170 mm^3, mice were intravenously injected by ARC with a dosage of 20 mg/kg. Another dose was administrated 3 days after the first dose. Tumor volume and body weight were measured every 2 days. When the tumor volume of the PBS group reached approximately 1500 mm^3, mice were euthanized. The tumor growth curves were plotted in GraphPad Prism 9.3.0.

Statistical Analysis. Statistical analysis was performed using GraphPad Prism 9.3.0, data were presented as mean ± standard deviation, *P*-values were calculated using the two-way

https://doi.org/10.1021/acs.bioconjchem.5c00212
Bioconjugate Chem. XXXX, XXX, XXX−XXX

ANOVA with Tukey's multiple comparison test, and $P < 0.05$ was considered to be statistically significant.

■ ASSOCIATED CONTENT

Supporting Information

The Supporting Information is available free of charge at https://pubs.acs.org/doi/10.1021/acs.bioconjchem.5c00212.

SEC chromatogram and SDS-PAGE gel image of ARCs; concentration-dependent gene silencing and cell binding by ARCs; siRNA stability test; in vivo gene silencing assay; antibody sequence information; additional experimental methods (PDF)

■ AUTHOR INFORMATION

Corresponding Author

Wanyi Tai − *Department of Pharmaceutical Engineering, School of Pharmaceutical Sciences, Wuhan University, Wuhan, Hubei 430071, China;* orcid.org/0000-0003-3589-8263; Email: wanyi-tai@whu.edu.cn

Authors

Yahui Liu − *Department of Pharmaceutical Engineering, School of Pharmaceutical Sciences, Wuhan University, Wuhan, Hubei 430071, China*

Yanan Quan − *Department of Pharmaceutical Engineering, School of Pharmaceutical Sciences, Wuhan University, Wuhan, Hubei 430071, China*

Qi Mao − *Department of Pharmaceutical Engineering, School of Pharmaceutical Sciences, Wuhan University, Wuhan, Hubei 430071, China*

Ruolin Xu − *Department of Pharmaceutical Engineering, School of Pharmaceutical Sciences, Wuhan University, Wuhan, Hubei 430071, China*

Complete contact information is available at: https://pubs.acs.org/10.1021/acs.bioconjchem.5c00212

Notes

The authors declare no competing financial interest.

■ ACKNOWLEDGMENTS

This work was financially supported by the National Key R&D Program of China (Grant No. 2021YFA0909900) and the National Natural Science Foundation of China (Grant No. 82273860).

■ REFERENCES

(1) Maier, M. A.; Jayaraman, M.; Matsuda, S.; Liu, J.; Barros, S.; Querbes, W.; Tam, Y. K.; Ansell, S. M.; Kumar, V.; Qin, J.; et al. Biodegradable lipids enabling rapidly eliminated lipid nanoparticles for systemic delivery of RNAi therapeutics. *Mol. Ther.* **2013**, *21* (8), 1570−1578.

(2) Wu, S. Y.; Lopez-Berestein, G.; Calin, G. A.; Sood, A. K. RNAi therapies: drugging the undruggable. *Sci. Transl. Med.* **2014**, *6* (240), No. 240ps7.

(3) Tang, Q.; Khvorova, A. RNAi-based drug design: considerations and future directions. *Nat. Rev. Drug Discovery* **2024**, *23* (5), 341−364.

(4) Wood, H. FDA approves patisiran to treat hereditary transthyretin amyloidosis. *Nat. Rev. Neurol.* **2018**, *14* (10), No. 570.

(5) Adams, D.; Gonzalez-Duarte, A.; O'Riordan, W. D.; Yang, C. C.; Ueda, M.; Kristen, A. V.; Tournev, I.; Schmidt, H. H.; Coelho, T.; Berk, J. L.; et al. Patisiran, an RNAi therapeutic, for hereditary transthyretin amyloidosis. *N. Engl. J. Med.* **2018**, *379* (1), 11−21.

(6) Xiao, B.; Wang, S.; Pan, Y.; Zhi, W.; Gu, C.; Guo, T.; Zhai, J.; Li, C.; Chen, Y. Q.; Wang, R. Development, opportunities, and challenges of siRNA nucleic acid drugs. *Mol. Ther. Nucleic Acids* **2025**, *36* (1), No. 102437.

(7) Guo, F.; Li, Y.; Yu, W.; Fu, Y.; Zhang, J.; Cao, H. Recent progress of small interfering RNA delivery on the market and clinical stage. *Mol. Pharmaceutics* **2024**, *21* (5), 2081−2096.

(8) Debacker, A. J.; Voutila, J.; Catley, M.; Blakey, D.; Habib, N. Delivery of oligonucleotides to the liver with GalNAc: from research to registered therapeutic drug. *Mol. Ther.* **2020**, *28* (8), 1759−1771.

(9) Akinc, A.; Querbes, W.; De, S.; Qin, J.; Frank-Kamenetsky, M.; Jayaprakash, K. N.; Jayaraman, M.; Rajeev, K. G.; Cantley, W. L.; Dorkin, J. R.; et al. Targeted delivery of RNAi therapeutics with endogenous and exogenous ligand-based mechanisms. *Mol. Ther.* **2010**, *18* (7), 1357−1364.

(10) Won Lee, J.; Kyu Shim, M.; Kim, H.; Jang, H.; Lee, Y.; Hwa Kim, S. RNAi therapies: expanding applications for extrahepatic diseases and overcoming delivery challenges. *Adv. Drug Delivery Rev.* **2023**, *201*, No. 115073.

(11) Sasso, J. M.; Tenchov, R.; Bird, R.; Iyer, K. A.; Ralhan, K.; Rodriguez, Y.; Zhou, Q. A. The evolving landscape of antibody−drug conjugates: in depth analysis of recent research progress. *Bioconjugate Chem.* **2023**, *34* (11), 1951−2000.

(12) Tai, W. Chemical modulation of siRNA lipophilicity for efficient delivery. *J. Controlled Release* **2019**, *307*, 98−107.

(13) Ripoll, M.; Cahuzac, H.; Dovgan, I.; Ursuegui, S.; Neuberg, P.; Erb, S.; Cianférani, S.; Kichler, A.; Remy, J. S.; Wagner, A. Supramolecular bioconjugation strategy for antibody-targeted delivery of siRNA. *Bioconjugate Chem.* **2024**, *35* (10), 1503−1511.

(14) Schneider, B.; Grote, M.; John, M.; Haas, A.; Bramlage, B.; Ickenstein, L. M.; Jahn-Hofmann, K.; Bauss, F.; Cheng, W.; Croasdale, R.; et al. Targeted siRNA delivery and mRNA knockdown mediated by bispecific digoxigenin-binding antibodies. *Mol. Ther. Nucleic Acids* **2012**, *1* (9), No. e46.

(15) Cuellar, T. L.; Barnes, D.; Nelson, C.; Tanguay, J.; Yu, S. F.; Wen, X.; Scales, S. J.; Gesch, J.; Davis, D.; van Brabant Smith, A.; et al. Systematic evaluation of antibody-mediated siRNA delivery using an industrial platform of THIOMAB-siRNA conjugates. *Nucleic Acids Res.* **2015**, *43* (2), 1189−1203.

(16) Nanna, A. R.; Kel'in, A. V.; Theile, C.; Pierson, J. M.; Voo, Z. X.; Garg, A.; Nair, J. K.; Maier, M. A.; Fitzgerald, K.; Rader, C. Generation and validation of structurally defined antibody-siRNA conjugates. *Nucleic Acids Res.* **2020**, *48* (10), 5281−5293.

(17) Cochran, M.; Arias, D.; Burke, R.; Chu, D.; Erdogan, G.; Hood, M.; Kovach, P.; Kwon, H. W.; Chen, Y.; Moon, M.; et al. Structure−activity relationship of antibody−oligonucleotide conjugates: evaluating bioconjugation strategies for antibody−siRNA conjugates for drug development. *J. Med. Chem.* **2024**, *67* (17), 14852−14867.

(18) Malecova, B.; Burke, R. S.; Cochran, M.; Hood, M. D.; Johns, R.; Kovach, P. R.; Doppalapudi, V. R.; Erdogan, G.; Arias, J. D.; Darimont, B.; et al. Targeted tissue delivery of RNA therapeutics using antibody-oligonucleotide conjugates (AOCs). *Nucleic Acids Res.* **2023**, *51* (12), 5901−5910.

(19) Sugo, T.; Terada, M.; Oikawa, T.; Miyata, K.; Nishimura, S.; Kenjo, E.; Ogasawara-Shimizu, M.; Makita, Y.; Imaichi, S.; Murata, S.; et al. Development of antibody-siRNA conjugate targeted to cardiac and skeletal muscles. *J. Controlled Release* **2016**, *237*, 1−13.

(20) Mullard, A. Antibody-oligonucleotide conjugates enter the clinic. *Nat. Rev. Drug Discovery* **2022**, *21* (1), 6−8.

(21) Xu, R.; Zheng, Y.; Tai, W. A single-chain fab derived drug conjugate for HER2 specific delivery. *Biomaterials* **2025**, *313*, No. 122798.

(22) Shen, B. Q.; Xu, K.; Liu, L.; Raab, H.; Bhakta, S.; Kenrick, M.; Parsons-Reponte, K. L.; Tien, J.; Yu, S. F.; Mai, E.; et al. Conjugation site modulates the in vivo stability and therapeutic activity of antibody-drug conjugates. *Nat. Biotechnol.* **2012**, *30* (2), 184−189.

(23) Song, S.; Liu, Y.; Liu, J.; Tai, W. In silico-driven THIOMAB approach for stable PROTAC conjugates by docking payloads in antibody cavities. *Bioconjugate Chem.* **2025**, *36* (36), 960−970.

(24) Marino, S. M.; Gladyshev, V. N. Analysis and functional prediction of reactive cysteine residues. *J. Biol. Chem.* **2012**, *287* (7), 4419−4425.
(25) Li, X.; Zhou, S.; Abrahams, C. L.; Krimm, S.; Smith, J.; Bajjuri, K.; Stephenson, H. T.; Henningsen, R.; Hanson, J.; Heibeck, T. H.; et al. Discovery of STRO-002, a novel homogeneous ADC targeting folate receptor alpha, for the treatment of ovarian and endometrial cancers. *Mol. Cancer Ther.* **2023**, *22* (2), 155−167.
(26) Zheng, Y.; Cheng, H.; Jiang, S.; Tai, W. Fc multisite conjugation and prolonged delivery of the Folate-targeted drug conjugate EC140. *Bioconjugate Chem.* **2025**, *36* (4), 762−769.
(27) Harumoto, T.; Iwai, H.; Tanigawa, M.; Kubo, T.; Atsumi, T.; Tsutsumi, K.; Takashima, M.; Destito, G.; Soloff, R.; Tomizuka, K.; et al. Enhancement of gene knockdown on CD22-expressing cells by chemically modified glycan ligand-siRNA conjugates. *ACS Chem. Biol.* **2022**, *17* (2), 292−298.
(28) Uehara, K.; Harumoto, T.; Makino, A.; Koda, Y.; Iwano, J.; Suzuki, Y.; Tanigawa, M.; Iwai, H.; Asano, K.; Kurihara, K.; et al. Targeted delivery to macrophages and dendritic cells by chemically modified mannose ligand-conjugated siRNA. *Nucleic Acids Res.* **2022**, *50* (9), 4840−4859.
(29) Dowdy, S. F.; Setten, R. L.; Cui, X. S.; Jadhav, S. G. Delivery of RNA therapeutics: the great endosomal escape! *Nucleic Acid Ther.* **2022**, *32* (5), 361−368.
(30) Dowdy, S. F. Overcoming cellular barriers for RNA therapeutics. *Nat. Biotechnol.* **2017**, *35* (3), 222−229.
(31) Prakash, T. P.; Allerson, C. R.; Dande, P.; Vickers, T. A.; Sioufi, N.; Jarres, R.; Baker, B. F.; Swayze, E. E.; Griffey, R. H.; Bhat, B. Positional effect of chemical modifications on short interference RNA activity in mammalian cells. *J. Med. Chem.* **2005**, *48* (13), 4247−4253.
(32) Nair, J. K.; Attarwala, H.; Sehgal, A.; Wang, Q.; Aluri, K.; Zhang, X.; Gao, M.; Liu, J.; Indrakanti, R.; Schofield, S.; et al. Impact of enhanced metabolic stability on pharmacokinetics and pharmacodynamics of GalNAc-siRNA conjugates. *Nucleic Acids Res.* **2017**, *45* (19), 10969−10977.
(33) Foster, D. J.; Brown, C. R.; Shaikh, S.; Trapp, C.; Schlegel, M. K.; Qian, K.; Sehgal, A.; Rajeev, K. G.; Jadhav, V.; Manoharan, M.; et al. Advanced siRNA designs further improve in vivo performance of GalNAc-siRNA conjugates. *Mol. Ther.* **2018**, *26* (3), 708−717.
(34) Takahashi, M.; Minakawa, N.; Matsuda, A. Synthesis and characterization of 2′-modified-4′-thioRNA: a comprehensive comparison of nuclease stability. *Nucleic Acids Res.* **2009**, *37* (4), 1353−1362.
(35) Brown, C. R.; Gupta, S.; Qin, J.; Racie, T.; He, G.; Lentini, S.; Malone, R.; Yu, M.; Matsuda, S.; Shulga-Morskaya, S.; et al. Investigating the pharmacodynamic durability of GalNAc-siRNA conjugates. *Nucleic Acids Res.* **2020**, *48* (21), 11827−11844.
(36) Prakash, T. P.; Graham, M. J.; Yu, J.; Carty, R.; Low, A.; Chappell, A.; Schmidt, K.; Zhao, C.; Aghajan, M.; Murray, H. F.; et al. Targeted delivery of antisense oligonucleotides to hepatocytes using triantennary N-acetyl galactosamine improves potency 10-fold in mice. *Nucleic Acids Res.* **2014**, *42* (13), 8796−8807.
(37) Gilleron, J.; Querbes, W.; Zeigerer, A.; Borodovsky, A.; Marsico, G.; Schubert, U.; Manygoats, K.; Seifert, S.; Andree, C.; Stöter, M.; et al. Image-based analysis of lipid nanoparticle−mediated siRNA delivery, intracellular trafficking and endosomal escape. *Nat. Biotechnol.* **2013**, *31* (7), 638−646.
(38) Humphreys, S. C.; Thayer, M. B.; Campuzano, I. D. G.; Netirojjanakul, C.; Rock, B. M. Quantification of siRNA-antibody conjugates in biological matrices by triplex-forming oligonucleotide ELISA. *Nucleic Acid Ther.* **2019**, *29* (3), 161−166.
(39) Fahs, S.; Lujan, P.; Köhn, M. Approaches to study phosphatases. *ACS Chem. Biol.* **2016**, *11* (11), 2944−2961.
(40) Cilliers, C.; Menezes, B.; Nessler, I.; Linderman, J.; Thurber, G. M. Improved tumor penetration and single-cell targeting of antibody-drug conjugates increases anticancer efficacy and host survival. *Cancer Res.* **2018**, *78* (3), 758−768.
(41) van Dongen, G. Improving tumor penetration of antibodies and antibody-drug conjugates: taking away the barriers for trojan horses. *Cancer Res.* **2021**, *81* (15), 3956−3957.
(42) Lu, G.; Nishio, N.; van den Berg, N. S.; Martin, B. A.; Fakurnejad, S.; van Keulen, S.; Colevas, A. D.; Thurber, G. M.; Rosenthal, E. L. Co-administered antibody improves penetration of antibody-dye conjugate into human cancers with implications for antibody-drug conjugates. *Nat. Commun.* **2020**, *11* (1), No. 5667.
(43) Sela, T.; Mansø, M.; Siegel, M.; Marban-Doran, C.; Ducret, A.; Niewöhner, J.; Ravn, J.; Martin, R. E.; Sommer, A.; Lohmann, S.; et al. Diligent design enables antibody-ASO conjugates with optimal pharmacokinetic properties. *Bioconjugate Chem.* **2023**, *34* (11), 2096−2111.
(44) Rocca, C.; Dennin, S.; Gu, Y.; Kim, J.; Chigas, S.; Najarian, D.; Chong, S.; Gutierrez, S.; Butler, J.; Charisse, K.; et al. Evaluation of electrophoretic mobility shift assay as a method to determine plasma protein binding of siRNA. *Bioanalysis* **2019**, *11* (21), 1927−1939.
(45) Gaus, H.; Miller, C. M.; Seth, P. P.; Harris, E. N. Structural determinants for the interactions of chemically modified nucleic acids with the Stabilin-2 clearance receptor. *Biochemistry* **2018**, *57* (14), 2061−2064.
(46) Tseng, Y. C.; Mozumdar, S.; Huang, L. Lipid-based systemic delivery of siRNA. *Adv. Drug Delivery Rev.* **2009**, *61* (9), 721−731.
(47) Mrksich, K.; Padilla, M. S.; Mitchell, M. J. Breaking the final barrier: Evolution of cationic and ionizable lipid structure in lipid nanoparticles to escape the endosome. *Adv. Drug Delivery Rev.* **2024**, *214*, No. 115446.
(48) Tai, W.; Gao, X. Functional peptides for siRNA delivery. *Adv. Drug Delivery Rev.* **2017**, *110−111*, 157−168.
(49) Wang, Y.; Huang, L. A window onto siRNA delivery. *Nat. Biotechnol.* **2013**, *31* (7), 611−612.
(50) He, C.; Migawa, M. T.; Chen, K.; Weston, T. A.; Tanowitz, M.; Song, W.; Guagliardo, P.; Iyer, K. S.; Bennett, C. F.; Fong, L. G.; et al. High-resolution visualization and quantification of nucleic acid-based therapeutics in cells and tissues using Nanoscale secondary ion mass spectrometry (NanoSIMS). *Nucleic Acids Res.* **2021**, *49* (1), 1−14.
(51) Springer, A. D.; Dowdy, S. F. GalNAc-siRNA conjugates: leading the way for delivery of RNAi therapeutics. *Nucleic Acid Ther.* **2018**, *28* (3), 109−118.

https://doi.org/10.1021/acs.bioconjchem.5c00212
Bioconjugate Chem. XXXX, XXX, XXX−XXX